Late Pliocene upwelling in the Southern Benguela region

Benjamin Petrick[1], Erin L. McClymont[2], Sonja Felder[1], Gemma Rueda[3], Melanie J. Leng[4,5], Antoni Rosell-Melé[3,6]

1. School of Geography, Politics & Sociology, Newcastle University, Claremont Road, Newcastle upon Tyne, NE1 7RU, UK.

2. Department of Geography, Durham University, South Road, Durham, DH1 3LE, UK.

3. Institut de Ciència i Tecnologia Ambientals (ICTA), Universitat Autònoma de Barcelona, Bellaterra, 08193, Spain.

4. NERC Isotope Geosciences Facilities, British Geological Survey, Keyworth, Nottingham, NG12 5GG, UK.

5. Centre for Environmental Geochemistry, University of Nottingham, Nottingham, NG7 2RD, UK.

6. ICREA, Barcelona, 08010, Spain.

19   **Abstract**

20   The Late Pliocene has been proposed as a possible analogue for understanding future

21   climate change and for testing climate models. Previous work has shown that during the

22   Pliocene the major upwelling systems were relatively warm, and that this meant they were

23   either inactive, contracted, or were upwelling warmer waters than present. Here, we examine

24   evidence from a site located on the margins of the modern Benguela Upwelling system to test

25   whether the upwelling cells had migrated or contracted relative to present during the Pliocene.

26   We applied several organic geochemistry proxies and foraminiferal analyses to

27   reconstruct the Pliocene history of ODP Site 1087 (31º28'S, 15º19'E, 1374m water depth),

28   including the $U^{K}_{37'}$ and TEX_{86} indices (for reconstructing sea surface temperatures),

29   phytoplankton biomarkers concentrations and stable isotope ratios (for estimating export

30   primary productivity, and for oxygen isotope statigraphy), and planktonic foraminifera

31   assemblage abundances (for inferring water mass changes). These proxies show that, between

32   3.5 and 3.0 Ma, the southern Benguela region was cooler than the northern Benguela region by

33   5°C, the latter being where the main upwelling cells are found today. From the multiproxy data

34   obtained, we also infer that more extensive upwelling was present in the southern Benguela

35   region during the Pliocene than at present, and that the Benguela Upwelling cells shifted

36   northwards after the Pliocene epoch as a result of changes in the local wind field. We also find

37   evidence that the Benguela Upwelling was sensitive to the pronounced cooling during the M2

38   and KM2 glacial stages, potentially associated with the expansion of sea ice and cooling in

39   Antarctica in the Late Pliocene.

40   Keywords: Pliocene, Benguela Upwelling, Agulhas Leakage, M2, Antarctica, Southern

41   Hemisphere, alkenones, GDGTs, foraminifera

42   **1. Introduction**

2

The Late Pliocene warm period, or the late Piacenzian, occurred between 3.3-3.0 Ma (Dowsett et al., 2012). This period has been studied extensively as a possible climate analogue for future warming (Dowsett et al., 1996), as climate conditions might have been similar to those predicted for the end of this century (IPCC, 2014). For instance, atmospheric CO_2 concentrations during the Late Pliocene have been reconstructed to be up to 450 ppmv, and thus lie close to those of end of 21st century climate predictions (Dowsett et al., 1996, 2012; Dowsett and Robinson, 2009; Henderiks and Pagani, 2007; Martínez-Botí et al., 2015; Seki et al., 2010) Within the overall warmth of the Pliocene, a pronounced excursion in the benthic $\delta^{18}O$ record marks the "M2 glaciation" at 3.3 Ma, which is seen as an early major cooling in global climate before the later onset of Northern Hemisphere glaciation from 2.6 Ma (De Schepper et al., 2009; Prell, 1984). To understand the climate system response to a warmer, higher CO_2 world (and the cooling events within this warm state), it is important to examine the evidence for regional and local responses in circulation change and biological productivity.

It is thought that during the Pliocene the major coastal and equatorial upwelling systems were either diminished in intensity, not present, or had a radically different mode of operation although more recent model reconstructions suggest an intensification of upwelling with future warmer temperatures (Brierley and Fedorov, 2010; Dekens et al., 2007; Etourneau et al., 2010, 2009; Fedorov et al., 2010; Harvey, 2000; Leduc et al., 2014; Rosell-Melé et al., 2014; Wang et al., 2015). The Benguela Upwelling system is one of the major upwelling cells in the modern global ocean (Boebel et al., 2003). It is located in the southeast Atlantic (Figure 1), and is divided into two regions: perennial upwelling in the northern and central Benguela, and seasonal upwelling in the southern Benguela (Boebel *et al.*, 2003). Previous work on the Pliocene-Pleistocene history of the Benguela Upwelling has focused on the northern and central Benguela region (Etourneau et al., 2010, 2009; Leduc et al., 2014; Marlow et al., 2001; Rosell-Melé et al., 2014), but less is known about the southern region. In the modern ocean,

3

68 waters offshore of the southern Benguela are also influenced by the intensity of the Agulhas

69 Leakage, which brings warm and salty Indian Ocean waters into the Atlantic, playing a key

70 role in heat and salt transport through the global ocean system (Beal et al., 2011; Gordon et al.,

71 1992; Weijer et al., 2001). Model reconstructions suggest that the Agulhas Leakage could have

72 been more vigorous during past warmer climates, and located in a similar position as today

73 (McKay et al., 2012). However, other studies suggest a diminished Agulhas Leakage during

74 the Pliocene because of reduced Indonesian Throughflow, which ultimately feeds the Agulhas

75 Current (Karas et al., 2011a, 2011b).
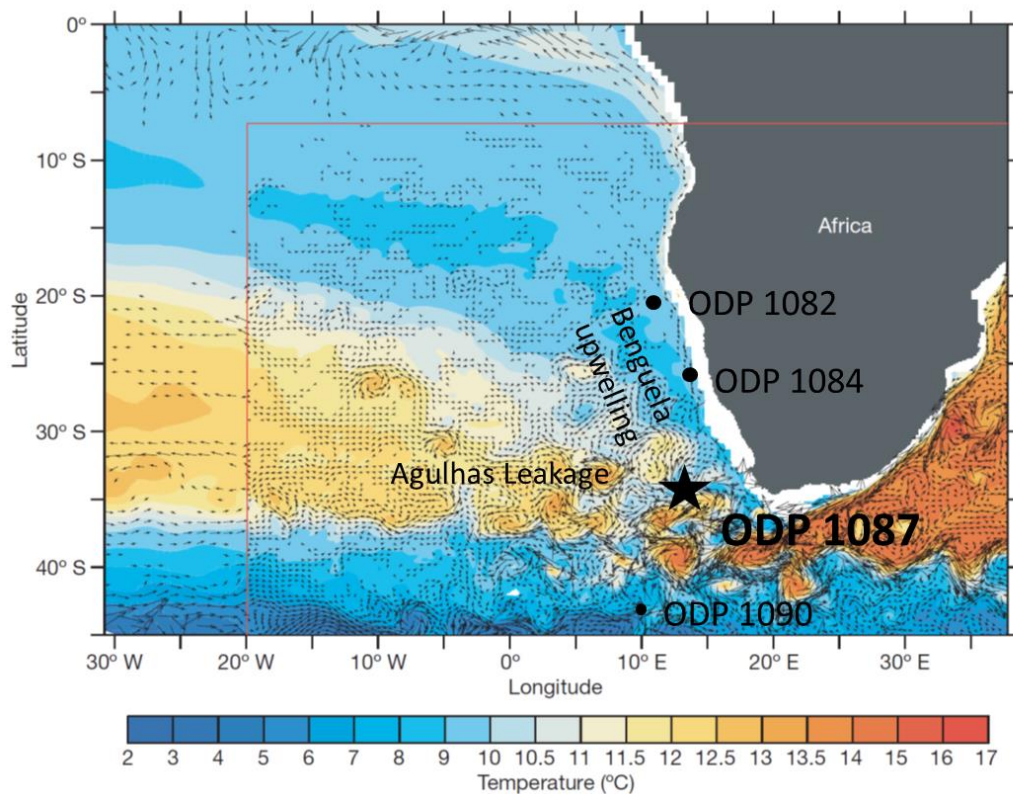
77 **Figure 1. Location map.** Location of the core site (ODP 1087) on a SST and surface ocean map of
78 SST (Colors) and current strength and position (arrows) (Biastoch et al., 2008). The location of local
79 Pliocene records and the location of major oceanic systems in their modern day positions are shown.

80

4

81   Here, we aim to explore changes in the local hydrography in the southeast Atlantic

82   Ocean during the Late Pliocene, by reconstructing SSTs, export productivity, and surface water

83   masses from 3.5 to 3.0 Ma at Ocean Drilling Program (ODP) site 1087, which is located

84   offshore of the modern southern Benguela Upwelling system (Figure 1). We apply two

85   biomarker proxies to estimate sea surface temperatures (SSTs): the U^K_{37}' and TEX_{86} indices

86   (Müller et al., 1998; Schouten et al., 2002). Chlorin pigment concentration mass accumulation

87   rates (MAR) (Rosell-Melé and Maxwell, 1996) and MAR of alkenones (Marlowe et al., 1984;

88   Volkman et al., 1980) are used to identify changes in export productivity. Planktonic

89   foraminifera assemblages are used to track the presence of Benguela and/or Agulhas waters, as

90   each water mass has distinctive species (Lee et al., 2008; Peeters et al., 2004; Ufkes and Kroon,

91   2012; Ufkes et al., 2000). Stable isotope ratios ($\delta^{18}O$, $\delta^{13}C$) of benthic foraminifera and <225

92   μm fraction carbonate provide insight into the structure of the water column. In combination,

93   these proxies allow us to investigate the signature of Benguela Upwelling and/or Agulhas

94   Leakage to the Southeast Atlantic during the Pliocene.

95   **2 Methods**

96   *2.1 Site description*

97   ODP Site 1087 (31º28'S, 15º19'E, 1374 m water depth) was drilled during ODP Leg

98   175, the goal of which was to investigate the history of the Benguela Upwelling system.

99   However, Site 1087 was drilled south of the major upwelling cells, with the aim of examining

100   changes in the Agulhas Leakage (Shipboard Scientific Party and Party, 1998). In this study,

101   samples were taken every 12 cm throughout the Late Pliocene, using the initial shipboard age

102   model (Shipboard Scientific Party, 1998). The age model was subsequently refined using the

103   stable isotope data, as described below, and samples were then taken every 4 cm between 3.5

104   and 3.0 Ma, to achieve an average sample resolution of 3 kyr.

5

105   *2.2 Biomarkers*

106   The biomarkers (alkenones, glycerol dialkyl glycerol tetraethers or GDGTs, and

107   chlorin pigments) were extracted from homogenised, freeze-dried sediment using a CEM

108   microwave system with 12ml of DCM:MeOH (3:1, v/v). Internal standards were added for

109   quantification (5α-cholestane, dotriacontane and tetracontane). The microwave temperature

110   programme heated samples to 70°C over 5 minutes, held at 70°C for 5 minutes and then

111   cooled down over 30 minutes (Kornilova and Rosell-Mele, 2003). The supernatant was then

112   decanted into vials, and the extracts were dried under a gentle stream of nitrogen. An aliquot

113   was taken for chlorins and GDGTs analyses. The remainder was derivatised using N,O-

114   bis(trimethlsiyl)trifluoroacetamide with trimethylchorosilane at 70°C for 1 hour prior to be

115   analysed to quantify alkenones using a gas chromatograph fitted with a flame-ionisation

116   detector (GC-FID) and a 30m HP1-MS capillary column. The injector temperature was held

117   at 300°C, and the detector at 310°C. The oven program was as follows: after injection, hold at

118   60 °C for 1 min, increase to 120°C at 20°C m^{-1}, to 310°C at 6°C m^{-1}, and hold at 310°C for 30

119   min. The U^{K}_{37}' was calculated using the relative abundances of the $C_{37:3}$ and $C_{37:2}$ alkenones

120   (Prahl and Wakeham, 1987), and converted to SSTs using the Müller et al. (1998) calibration.

121   The total alkenone concentrations were determined by reference to the internal standard

122   mass, and then converted to alkenone MAR using the new linear sedimentation rates and the

123   shipboard dry bulk density measurements (Shipboard Party 1998), following the approach of

124   Emeis et al. (1995).

125   Based on the results from the U^{K}_{37}' analysis, a subset of 20 samples was selected for

126   further investigation using the TEX^{H}_{86} index. An aliquot of the total extract was separated into

127   different compound classes using silica column chromatography (5% H_2O) and eluted with

128   solvents of increasing polarity: Fraction 1 (hexane), Fraction 2 (dichloromethane; alkenones)

129   and Fraction 3 (methanol; GDGTs). All fractions were dried under a stream of N_2. Fraction 3

130 was re-dissolved in 200 μl of hexane:*n*-propanol (98.5:1.5, v/v) and an internal standard (GR)

131 was added to the sample, which was filtered through a 0.5 μm PTFE filter. The filtered samples

132 were analysed by high performance liquid chromatography - mass spectrometry (HPLC-MS),

133 using a Dionex P680 HPLC coupled to a Thermo Finnigan TSQ Quantum Discovery Max

134 quadrupole MS, with an atmospheric pressure chemical ionization (APCI) interface set in

135 positive mode. Instrumental and chromatographic conditions were adopted from Fietz et al.

136 (2011). GDGTs were detected in selected ion monitoring (SIM) mode at the following mass to

137 charge ratio (m/z): 1302, 1300, 1298, 1296, 1292, 1050, 1048, 1046, 1036, 1034, 1032, 1022,

138 1020, 1018, and the internal standard GR at 1208 m/z. TEX^H_{86} was calculated using the relative

139 abundances of GDGT I, GDGT II, GDGT III and Crenarchaeol based on the methodology by

140 Kim et al. (2010).

141 Chlorins were analysed using an HPLC system coupled to a photo-diode array

142 spectrophotometer (PDA) in offline mode. An aliquot of the original solvent extract was

143 dissolved in 2 mL of acetone, and 40 μL was injected into the HPLC. The absorbance at the

144 410 nm wavelength was used to calculate, in triplicate measurements, mean chlorin pigments

145 concentration per sample. Analytical variability was monitored using repeated measurements

146 of a standard, and was determined at 0.07 absorbance units. Finally, for all samples, the chlorin

147 concentration at 410 nm was divided by the original weight of the total sample to get a value

148 of absorbance per gram; chlorin pigments MAR was calculated following the approach

149 outlined above for alkenone MAR.

150 *2.3 Foraminifera assemblages and stable isotopes*

151 For foraminiferal stable isotope analysis, 80 samples (12 cm resolution) of

152 approximately 5 cc of sediment were washed though a 150 μm sieve. The >150 μm fraction

153 was dried in a 40°C oven and examined under a binocular microscope to identify and pick 3–

154 8 *Cibicidoides wuellerstorfi* benthic foraminifera (BF) tests.

7

155   Due to a lack of *C. wuellerstorfi* tests in some samples, stable isotope analysis on <225

156   μm fraction carbonate (fine fraction) were undertaken, using a second set of 87 5 cc samples

157   at 4 cm resolution. The <225 μm fraction (mostly represented by coccoliths) was collected

158   using 0.5 μg sieves.

159   Approximately 30-100 μg of carbonate (fine fraction FF, or benthic foraminifera BF)

160   were analysed for stable isotope ratios using an IsoPrime dual inlet mass spectrometer plus

161   Multiprep device. Isotope rations ($\delta^{18}O$ and $\delta^{13}C$) are reported as per mille (‰) deviations of

162   the isotopic ratios ($^{18}O/^{16}O$ and $^{13}C/^{12}C$) calculated to the VPDB scale using a within-run

163   laboratory standard (KCM) calibrated against NBS-19. Analytical reproducibility of KCM is

164   < 0.1‰ for $\delta^{18}O$ and $\delta^{13}C$.

165

166   The >225 μm fraction was retained and 14 samples were selected for planktonic foraminifera

167   analysis, guided by the U^{K}_{37}' and chlorin data. The assemblage samples were passed through

168   a 125 μm sieve Because of the location of ODP site 1087 is close to the polar front and

169   Benguela upwelling the fraction >125 microns, rather than >150 microns was used to pick

170   foraminifera. In polar and upwelling regions, it is better to study assemblages in the >125

171   microns to cover all adult forms of planktonic foraminifera, as they tend to be smaller in cold

172   waters masses (Stephan Steinke, MARUM, personal communication in 2011). The samples

173   were also chosen to replicate studies that had been previously done at this site (Giraudeau,

174   1993; Giraudeau et al., 2001; Pierre et al., 2001). For each sample, 300 to 410 foraminifera

175   were picked in order to reflect the total diversity of the foraminifera. Percentages of individual

176   species vs. total number of foraminifera counted were calculated and subcategories of

177   abundances formed as follows: dominant (>40% of total assemblage), abundant (20-40%), few

178   (10-20%), rare (4-10%), present (<4%).

179

3. Results

3.1 Age model

According to the shipboard age models (Shipboard Scientific Party, 1998), the Late Pliocene occurred after 147 mcd, which was located using the Mammoth magnetic reversal at 3.33 Ma. The low resolution (12 cm) isotopic? analysis of the benthic foraminifer *C. wuellerstorfi* ($\delta^{18}O_{BF}$) was able to identify several key excursions, as detailed in the benthic $\delta^{18}O$ stack, LR04 (Lisiecki and Raymo, 2005), including 'KM2', which is considered to be one of the coldest stages during the Pliocene (De Schepper et al., 2009; Dwyer and Chandler, 2009; Passchier, 2011) (Figure 2c). To supplement the $\delta^{18}O_{BF}$ record, we followed the approach of Dickson et al. (2010), developed using a proximal core (ODP Site 1085), by using $\delta^{18}O_{FF}$ (carbonate <225 µm) (Figure 2d). The $\delta^{18}O_{FF}$ record includes changes in surface ocean temperature and salinity; however, Dickson et al. (2010) showed that there is a close relationship between $\delta^{18}O_{FF}$ and $\delta^{18}O_{BF}$ in the Southern Benguela region, which allows for orbitally-tuned age model construction, especially where there is a fragmentary $\delta^{18}O_{BF}$ record.
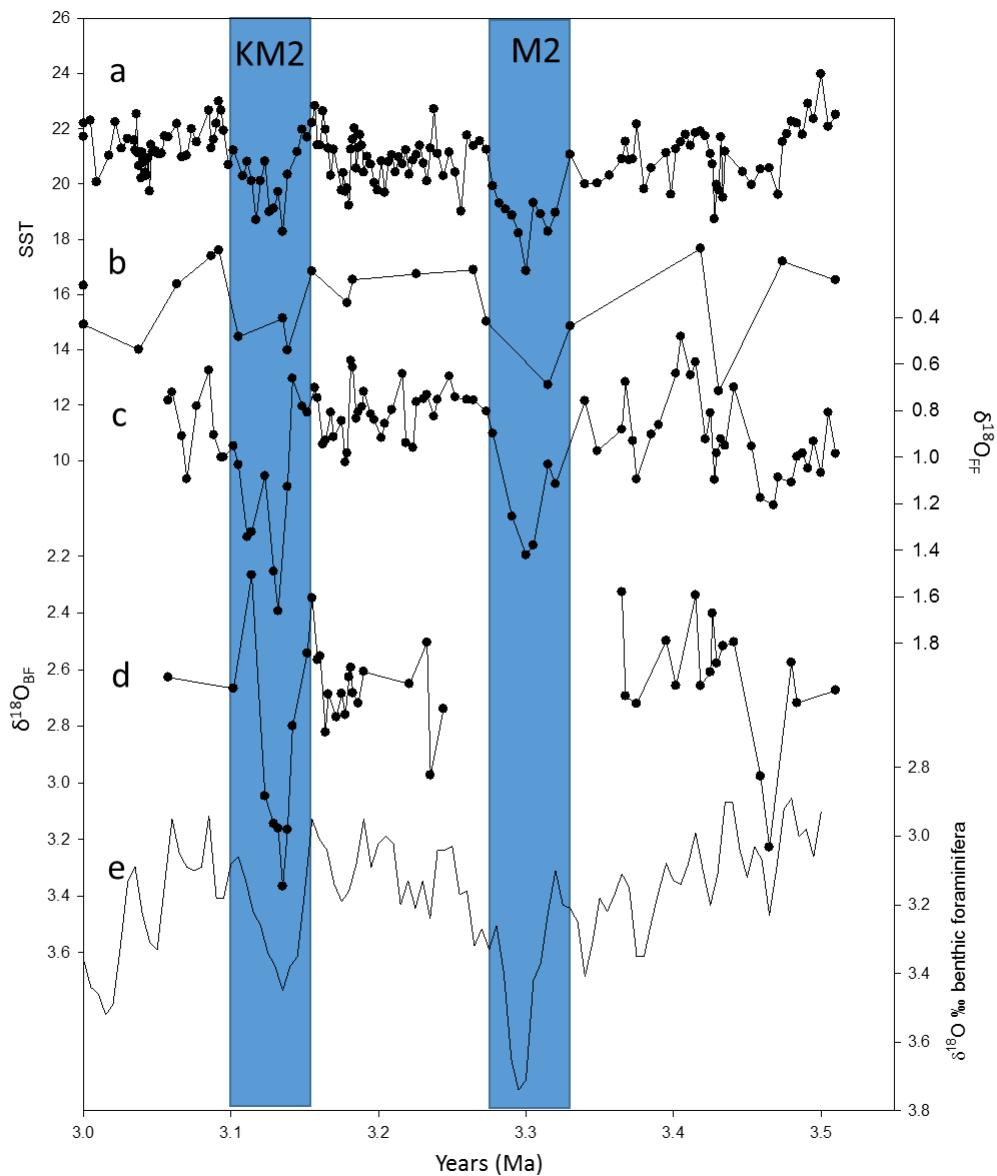
Figure 2. Late Pliocene temperature and stable isotope records from ODP Site 1087 plotted against the new benthic $\delta^{18}O$ stratigraphy. The two major cold periods in the records are marked by vertical blue bars. a) $U^{K}_{37}{}'$ SSTs calculated using the calibration of Muller et al. (1998), b) TEX^{H}_{86} temperatures determined using the calibration of Kim et al. (2010); c) $\delta^{18}O_{FF}$; d) record of $\delta^{18}O_{BF}$ re-tuned to the LR04 global benthic $\delta^{18}O$ stack (Lisiecki and Raymo, 2005); and d) LR04 global benthic $\delta^{18}O$ stack.

The $\delta^{18}O_{FF}$ record from ODP Site 1087 was visually tuned to LR04 using the two major cold periods (M2, KM2) as tie points to fix the age model (Figure 2). The age uncertainty in the tuning component of the age model is ~10 ka based on multiple tuning attempts for the finer scale tuning. The comparison between the $\delta^{18}O_{FF}$ and $\delta^{18}O_{BF}$ shows that the offset

10

205 between the two records (where enough data existed to compare) is at most 4 ka, although for

206 most of the time it is less than 1 ka, and there is no consistent lead or lag between them. The

207 timing of the large positive excursion in benthic $\delta^{18}O$ marking the "M2 glaciation" at 3.30 Ma

208 is close to the timing of the Mammoth magnetic excursion previously identified at 147 mcd at

209 3.33 Ma (Shipboard Scientific Party, 1998), giving confidence in the $\delta^{18}O$ age model. The

210 remainder of the record was tuned to LR04 using both the $\delta^{18}O_{BF}$ and $\delta^{18}O_{FF}$ data.

211 *3.2 Temperature*

212   The U^{K}_{37}' values between 3.0 and 3.5 Ma range between 0.59 and 0.83, which convert

213 to an SST range of 17 to 22.5°C (mean SST is 21°C) (Figure 2a). There are two prominent cold

214 periods in the record. The first occurs between 3.32 and 3.26 Ma (the M2 stage), when SSTs

215 are between 16.5 and 19°C. The second major cooling occurs between 3.15 and 3.10 Ma

216 (KM2), with SSTs ranging between 18 and 21°C.TEX^{H}_{86} temperatures ranged from 13 to 17.5

217 °C with a mean of 15 °C (Figure 2b). The TEX^{H}_{86} temperature minima are found at 3.4 Ma (13

218 °C), during M2 (13 °C) (3.3 Ma) and around 3.05 Ma (14 °C) during KM2. There is a

219 discrepancy of aproxmently °C.   This offset is consistent throughout the entire record.

220 *3.3 Other biomarkers*

221   The mean total alkenone concentration is 25.53 µg g^{-1} (range: 14.9-51.5 µg g^{-1}). The

222 average alkenone MAR is 2.43 (range: 0.67-5.59 µg (yr cm^2)$^{-1}$; Figure 3b). The three highest

223 values occurred before 3.30 Ma, when the range of values is high. After 3.30 Ma, average

224 alkenone MAR falls, and the range of MAR values is much reduced.

11

225
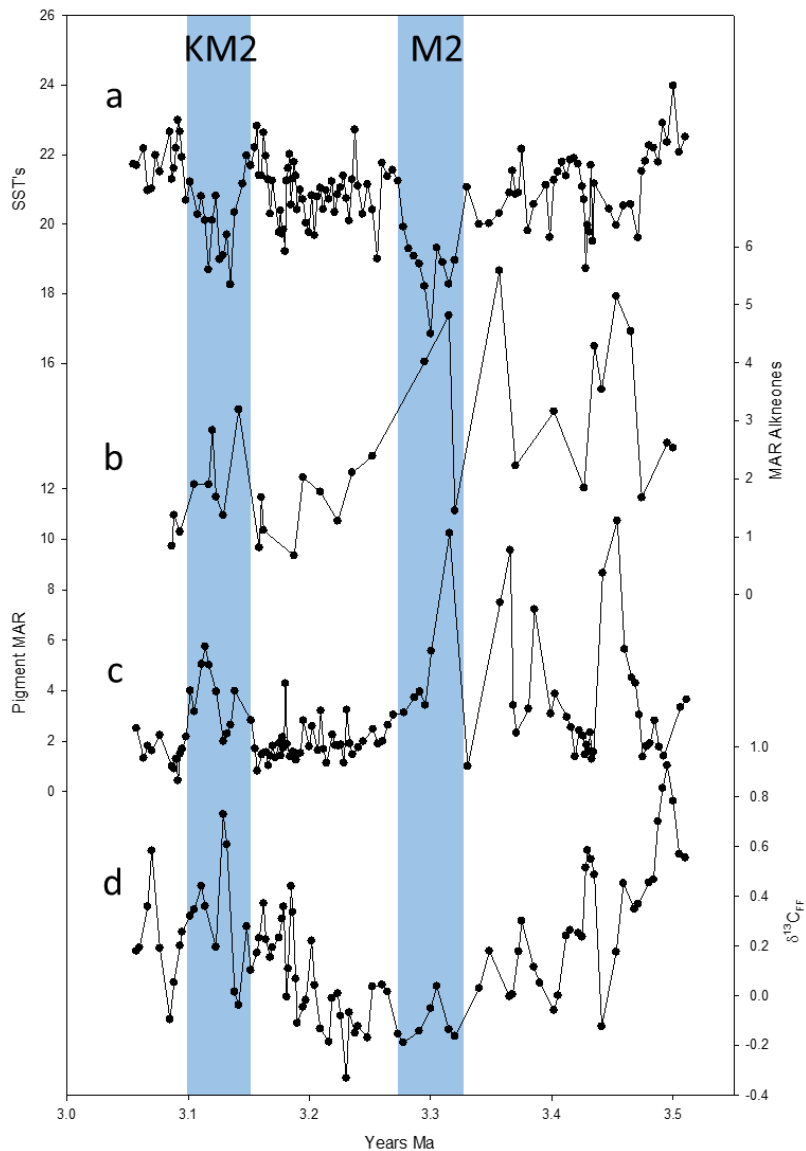
Figure 3 SSTs and indicators of export production from ODP Site 1087. The two major cold periods are marked by blue bars. a) U^K_{37}' SSTs calculated using the calibration of Muller et al. (1998); b) Total C_{37} alkenone mass accumulation rates (MAR); c) Chlorin pigments MAR (410 nm). d) $\delta^{13}C$ <225 μm fraction .

Total chlorin concentrations range between 0.09 and 0.73 abs g^{-1}; chlorin MAR range between 0.4-18.25 g^2 (yr cm^2 abs)$^{-1}$.. There is greater variability and a higher overall mean in chlorin concentration and MAR prior to 3.30 Ma. In general, chlorin and alkenone MARs increase when U^K_{37}', TEX^H_{86} indices indicate cold SSTs. (Figure 3c).

3.5 Stable isotope records: <225 μm fraction and benthic foraminifera carbonate

236   The mean $\delta^{18}O_{FF}$ is +1.0‰ (range = +1.6‰ to +0.5‰, Figure 2c). There are two

237   increases in $\delta^{18}O_{FF}$ centred on 3.3 and 3.1 Ma, where $\delta^{18}O$ exceeds +1.4‰. The mean $\delta^{13}C_{FF}$

238   is 0.2‰ (range = +0.9‰ to –0.3‰, Figure 3d). The $\delta^{13}C_{FF}$ shows a long-term decrease by 1

239   ‰ from 3.5 to 3.3 Ma.   The $\delta^{13}C_{FF}$ then increases by around 0.7‰ from 3.3 to 3.0 Ma. It has

240   been shown that the fine fraction carbonate at the site is dominated by coccoliths (McClymont

241   et al., 2005), so it is assumed that the <225 μm fraction record is dominated by coccoliths and

242   that the isotopes reflect changes from the original coccolithophores. The influences on the

243    $\delta^{13}C_{FF}$ are complex and there are few $\delta^{13}C$ studies on coccoliths (Ziveri et al., 2003). However,

244   the few studies that have been done seem to indicate a higher $\delta^{13}C$ signature during times of

245   higher productivity (Malinverno et al., 2008; Ziveri et al., 2003).   This also fits the

246   interpretation of the $\delta^{13}C$ from foraminifera previously studied at this site (Pierre et al., 2001).

247   Therefore it is assumed that at least part of the $\delta^{13}C_{FF}$ record is influenced by changes in

248   productivity.

249   The $\delta^{18}O_{BF}$ shows broadly similar trends to the $\delta^{18}O_{FF}$ (Figure 2d). There are positive

250   isotope excursions centred on 3.1 Ma and 3.45 Ma. The gap in the $\delta^{18}O_{BF}$ around 3.3 Ma,

251   which lasts 115 ka, is due to the lack of *C. wuellerstorfi* preserved in this part of the record.

252   ***3.6 Planktonic foraminifera assemblages***

253   The mean percentages of the most common assemblages planktonic foraminifera change from

254   3.24 onwards (Table 1). Before 3.24 Ma, the majority of the identified planktonic foraminifera

255   are *Globigerinoides bulloides*, which is always either abundant or dominant, and *Globorotalia*

256   *inflata*, which is mainly classified as abundant. The only time when these two species do not

257   dominate the planktonic foraminifera assemblage is in the sample dated 3.25 Ma; here, *G.*

258   *inflata* is classified as rare although *G. bulloides* is still abundant. In contrast to the other

13

samples, *Neogloboquadrina pachyderma (sin)* is abundant in the sample at 3.25 Ma; although

it is usually less than 10% of the assemblage (few or rare abundance) for the remaining Pliocene

samples analysed here.

Age/ Species	3076.7	3085.0	3121.7	3135.0	3163.6	3170.7	3181.0	3217.0	3241.0	3283.9	3366.7	3403.2	3426.4	3467.5
G. inflata	A	A	A	A	F	A	D	F	A	R	D	D	A	A
G. glutinata	R	F	A	A	F	F	F	A	F	F	R	F	A	R
G. bulloides	A	A	A	A	A	A	A	A	D	A	A	D	A	D
G. ruber	R	P	x	R	P	x	R	P	P	P	R	R	R	F
N. pachy. (dex)	A	A	D	D	D	A	A	D	R	R	R	R	P	P
N. pachy. (sin)	F	R	R	R	F	R	R	R	F	A	R	R	F	F
G. siphonifera	P	P	x	P	P	x	x	P	P	P	P	x	P	x
G. falconensis	R	R	R	R	P	R	x	R	R	R	R	R	F	R
O. universa	P	R	P	x	P	R	x	P	x	x	P	P	P	P
G. menardii	P	R	x	R	P	x	x	x	x	P	P	x	x	P
G. conglobatus	x	R	P	x	P	P	R	x	R	x	x	x	P	x
G. quinqueloba	P	x	R	R	x	P	X	R	x	P	x	x	P	x
G. sacculifer	x	x	x	X	x	x	X	x	x	P	x	x	x	x

Table 1. Showing the abundance of major foraminifera through the record. Percentages of individual species vs. total number of foraminifera counted were calculated and subcategories of abundances formed: dominant (>40% of total assemblage D), abundant (20-40% A), few (10-20% F), rare (4-10% R), present (<4% P) and absent (X).

After 3.24 Ma, the majority of foraminifera are comprised of *G. bulloides*, *G. inflata,* and *N. pachyderma (dex)*. The abundant or dominant classification of *N. pachyderma (dex)* after 3.24 Ma is in contrast to its much lower contribution to the assemblage prior to 3.24 Ma. Minor contributions from several other species are noted throughout the Pliocene. *Globigerinoides ruber* is composed of less than 5% of the Pliocene assemblage except in the oldest sample. A small number of warm water (Indian Ocean) species (Peeters et al., 2004) occur in the Pliocene record from ODP Site 1087: *Globigerina falconensis* is present throughout, but is usually categorised as few (<5%). There are 7 samples where *Globorotalia menardii* are identified, although there are never more than 4 individuals per sample. *G. menardii* is another important Indian Ocean warm water species, and has been identified in

279   ODP Site 1087 and other southeast Atlantic sediment cores during the late Pleistocene (Caley

280   et al., 2012; Peeters et al., 2004; Sexton and Norris, 2011)

281   **4. Discussion**

282   *4.1 Pliocene conditions at ODP Site 1087*

283   At ODP Site 1087, the Late Pliocene is marked by an overall absence of any long-term

284   trends in SST, $\delta^{18}O_{FF}$ and $\delta^{18}O_{BF}$. However, there are trends in the alkenone and chlorin MAR,

285   which show shifts in variability halfway through the record at 3.30 Ma, and in $\delta^{13}C_{FF}$, which

286   shows an initial decreasing record and then an increasing record after 3.30 Ma. On orbital and

287   shorter timescales, the general relationships between the records shown in Figures 2 and 3 are

288   as follows: high SSTs (U^K_{37}' and TEX^H_{86}) are usually associated with low chlorin MAR, low

289   alkenone MAR and lower $\delta^{18}O_{FF}$, $\delta^{18}O_{BF}$ and relatively lower $\delta^{13}C_{FF}$. Periods of lower SST

290   (U^K_{37}' and TEX^H_{86}) are associated with higher chlorin and alkenone MAR and higher $\delta^{18}O_{FF}$

291   and $\delta^{18}O_{BF}$.

292   The most pronounced excursion in all of the data sets occurs during the time of the M2

293   glacial stage c. 3.30 Ma (Figures 2 and 3). There is a 5 ℃ drop in U^K_{37}'-SST, in tandem with

294   increases in $\delta^{18}O_{FF}$, chlorin MAR and alkenone MAR (Figure 3). Lower variability in chlorin

295   MAR and alkenone MAR and an increase in $\delta^{13}C_{FF}$ are also recorded after 3.30 Ma.

296   A second major cooling event occurs between 3.15 and 3.10 Ma, during the time of the

297   KM2 glacial stage (Figures 2 and 3). Many of the patterns observed during M2 are also

298   recorded here (low SST, higher export productivity). However, in contrast to M2, there is no

299   significant change in the planktonic foraminifera assemblage either during or after the cooling

300   event (Table 1). The $\delta^{18}O_{FF}$ shows a greater increase during this glacial period than during

301   M2, suggesting more cooling of the water, possibly coupled with fresher water.

15

4.2 Benguela Upwelling at ODP Site 1087

ODP Site 1087 is located offshore of the southern Benguela Upwelling cells at the present day. This location, in combination with the influence of Agulhas Leakage, keeps at present ODP Site 1087 warmer and less productive than the main Benguela Upwelling cells to the north and east (Boebel, 2003). Warmer-than-present Pliocene SSTs at ODP Site 1087, as determined here, could imply an increased Agulhas Leakage of warm waters into the SE Atlantic. However, Late Pliocene SSTs at ODP Site 1087 are colder than both at ODP sites 1082 and 1084, which lie beneath the northern and central cells of the upwelling at the present day (Figures 1 and 4) (Etourneau et al., 2009; Marlow et al., 2000; Rosell-Melé et al., 2014). This is an unexpected scenario if the Agulhas current, and its leakage, were more vigorous during the Late Pliocene. The relatively cool SSTs observed at ODP Site 1087 in the Pliocene, compared to the northern Benguela Upwelling cells, indicate that there was not a contribution of warmer water to the site, as is observed during periods of increased Agulhas Leakage in the late Pleistocene (Peeters et al., 2004). Furthermore, two species of primarily Indian Ocean foraminifera occur in low abundances at ODO Site 1087 during the Late Pliocene: *G. falconensis* (rare/present), used to identify Agulhas Leakage by Peeters et al., (2004), and *G. menardii* (rare/present) (Table 1). The latter species is particularly important because it is considered to be indicative of Agulhas Leakage during the late Pleistocene for ODP Site 1087 (Peeters et al., 2004; Caley et al., 2012), whereas it is only present (but rare) during times of inferred lower export productivity in the Pliocene at ODP Site 1087. The data from ODP Site 1087 thus suggest a reduced influence of Agulhas Leakage to the southeast Atlantic in the Late Pliocene. It is possible that the Agulhas Leakage occurred, but that it is not recorded at ODP Site 1087 because it was located further to the south overall. However, the evidence at ODP Site 1087 supports the proposal that the vigour and scope of the Agulhas current has increased since the Miocene to the Pleistocene (Diekmann *et al.*, 2003).

The absent or weak influence of Agulhas leakage at ODP Site 1087 during the Pliocene means that the oceanographic regime in the southeast Atlantic was different from the modern. TEX^H_{86} temperatures are always colder than those recorded by the U^K_{37}' index (Figure 2) , which has also been observed in the modern Benguela Upwelling system (Lee et al., 2008). In the modern upwelling cells, the Archaea producing GDGTs are interpreted to be found deeper in the water column due to higher nutrient availability (Lee et al., 2008). More recent studies have shown that there is a connection between increased nutrient supply in areas such as upwelling systems and offsets of temperatures between the TEX_{86} and U^K_{37}' because the increase in productivity may change the water depth at which GDGTs are predominatly produced (Hernández-Sánchez et al., 2014; Huguet et al., 2007; McClymont et al., 2012; Shaari et al., 2013). The U^K_{37}'-TEX_{86} offset during the Pliocene at ODP Site 1087 therefore may be interpreted to be a result of upwelling. Further support for the interpretation of higher amounts of upwelling comes from the higher export of chlorin and alkenones in the Pliocene compared to late Pleistocene values (Petrick 2014). Finally the foraminifera assemblage supports evidence for upwelling, given that the dominant foraminifera species (*G. inflata* and *N. pachyderma (dex)),* are prominent in the modern Benguela Upwelling system (Lee et al., 2008). *G. inflata* is indicative of the outer edges of the upwelling (Groeneveld and Chiessi, 2011), while *N. pachyderma (dex)* is found in the filaments produced by seasonal upwelling around the permanent upwelling cells (Ufkes et al., 2000; Ufkes and Kroon, 2012). The combined temperature, chlorin, alkenone, $\delta^{13}C_{FF}$ and foraminifera assemblage datasets indicate that during the Pliocene the southern Benguela Upwelling system was more extensive and/or less seasonal in nature, compared to its modern and late Pleistocene operation. Supporting our interpretation that ODP Site 1087 was affected by a southward displaced Benguela Upwelling system relative to present is that there is no expression of the M2 or of the KM2 glacial stages at the northern Benguela Site, ODP 1082 (Figure 4). This suggests that these cool, high

17

352 productivity (upwelling) events were isolated to the southern Benguela region, which was

353 likely controlled by (or sensitive to) different processes than the northern Benguela.
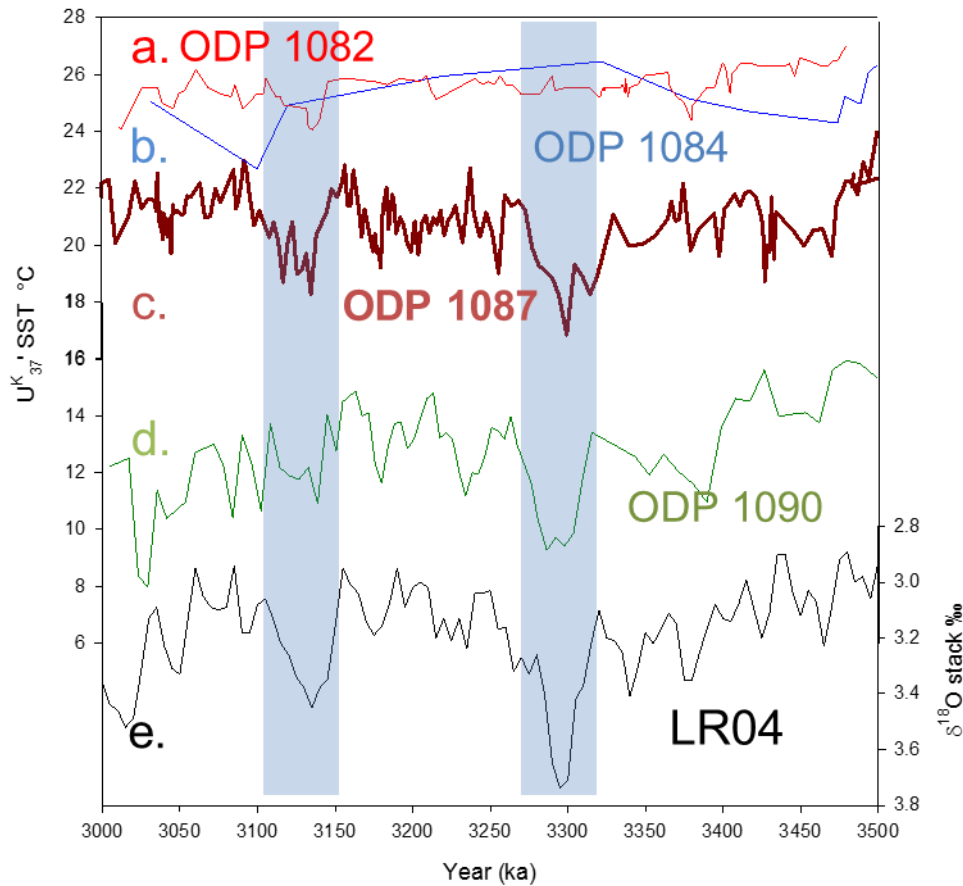
354

355 **Figure 4. Late Pliocene SSTs in the southeast Atlantic.** a) ODP1082 (red; Etourneau et al., 2009)
356 b. ODP 1084 (blue), (Marlow et al., 2000) c) ODP 1087 (dark red) (This study) d) ODP 1090 (Dark
357 green) (Martinez-Garcia et al., 2011). e) The LR04 Benthic stack (Black) is shown for reference
358 (Lisiecki and Raymo, 2005). Blue bars represent cold periods.

359

4.3 Changes in the Southeast Atlantic during the Pliocene

361   Decreasing SSTs and increasing productivity have been used to argue that the northern

362 and central upwelling cells of the Benguela system developed their modern form around 2.4-

363 2.0 Ma (Etourneau *et al.*, 2009,2010, 2012). The development of an SST gradient between

18

364 ODP sites 1081 and 1084 from 3.5 Ma (Figure 4) was interpreted by Rosell-Mele et al. (2014)

365 to indicate an earlier initial onset of Benguela Upwelling intensification (although still weaker

366 than modern), and was closely linked to increased dust accumulation in the Subantarctic

367 Atlantic, which reflects intensification of atmospheric circulation at this time (Martinez-Garcia

368 et al., 2011). Furthermore, recent studies show that upwelling may have been present in the

369 northern upwelling sites between 3.5 and 3.0 Ma; however, it was suggested that there was

370 fundamental difference between Pliocene upwelling and modern day upwelling based on the

371 change in the biomarkers seen in the early Pliocene (Leduc et al. 2014). Rosell-Mele et al.

372 (2014) interpreted the low SST gradient between ODP 1081 and 1084 to indicate a warm,

373 persistent 'Benguela El Niño-like' state for the region during the Pliocene (Rosell-Melé et al.

374 2014). Our results support this interpretation in principle, demonstrating that active upwelling

375 was present in the Pliocene, but that it was displaced southwards into the Southern Benguela

376 region relative to modern. This interpretation contrasts with earlier studies that have assumed

377 there was little Benguela Upwelling occurring before 3.0 Ma (Brierley and Fedorov, 2010;

378 Fedorov et al., 2007, 2010, 2006).

379 As a wind-driven system (Hutchings et al., 2009), the Pliocene displacement in the

380 Benguela Upwelling is likely related to a change in the position and/or intensity of atmospheric

381 circulation in the Southern Hemisphere compared to modern. Today, upwelling only affects

382 the southern part of the Benguela upwelling system during the austral summer due to the

383 southward expansion in the wind patterns, which are only seasonally active in this part of the

384 system, whereas perennial upwelling dominates the central and northern regions (Andrews and

385 Hutchings, 1980). However, during the Late Pliocene, it has been argued that the Hadley cells

386 were expanded 3-4 degrees of latitude southward (Brierley et al., 2009; Etourneau et al., 2010).

387 From 3.5 Ma, increased dust deposition to ODP Site 1090 (Martinez-Garcia et al., 2011) is

388 interpreted to reflect an intensification of atmospheric circulation in the southern hemisphere

19

389   and/or reduced precipitation in South America and Africa, both consistent with relatively weak

390   Hadley circulation (Brierley et al., 2009). A southward displacement of the trade winds would

391   have been conducive to the development of perennial upwelling in the southern Benguela

392   region (Christensen et al., 2002). The dominant proposal to explain the shifting and/or

393   strengthening Hadley circulation over the Pliocene and Pleistocene draws on the strengthening

394   of meridional temperature gradients which have evolved over this time window, particularly

395   clearly expressed in SST data sets (Brierley et al., 2009; Fedorov et al., 2010, 2006; Martinez-

396   Garcia et al., 2010). However, model sensitivity tests have recently demonstrated that the

397   intensity of the Benguela upwelling system could be impacted by tectonic uplift in the African

398   continent through the Miocene and Pliocene (Jung et al., 2014). For example, an intensification

399   of Ekman pumping in the Benguela region of up to 40-60% was demonstrated, due to altered

400   atmospheric circulation in response to uplift in southern and eastern Africa, but the potential

401   for strong regional differences was also indicated, e.g. between northern and southern Benguela

402   regions (Jung et al., 2014). It is currently difficult to assess whether this mechanism can explain

403   a southward displacement of the Benguela upwelling during the late Pliocene, as we suggest

404   here, since the timing and pattern of uplift in Africa remains controversial (see discussion by

405   Jung et al., 2014) and there is evidence for gradual cooling (and inferred upwelling

406   intensification) in the Peru upwelling system since 4 Ma (Dekens et al., 2007), which could not

407   be explained through an African uplift mechanism. Further work is required to constrain the

408   meridional SST gradients outside of the upwelling regions, as well as other indicators of Hadley

409   circulation changes, alongside improved chronologies of African uplift, in order to better assess

410   the relative importance of these different mechanisms in explaining the patterns observed in

411   the Pliocene Benguela upwelling system.

412   *4.4 Climate changes in the Southern Hemisphere from 3.30 Ma*

413   The decreases in chlorin MAR and alkenone MAR after the M2 glacial stage suggest a

414   change in the nature of the Benguela upwelling system through the late Pliocene (Figures 3).

415   M2 also marks an inflection point in the $\delta^{13}C_{FF}$ record, which shows a long-term rise after M2.

416   The planktonic foraminifera species distribution shows major changes during and after the M2

417   glacial stage. This is especially true of N. *pachyderma (sin.),* which shows a peak during M2

418   and N. *pachyderma (dex.),* which increases after 3.3 Ma (Table 1). Both of these species are

419   associated with the Benguela upwelling in the modern system (Giraudeau et al., 2002, 2001;

420   Ufkes and Kroon, 2012; Ufkes et al., 2000). While this is based on low resolution samples, it

421   fits the patterns seen in the higher resolution geobiological data, by showing a major shift in

422   the environment of the upwelling after M2. The M2 stage at ODP Site 1087 is therefore

423   important in marking a shift in the nature of the organic depotion at ODP Site 1087.

424   The M2 glacial stage has also been described as being an important marker of long-

425   term shifts in southern hemisphere climate (Lisiecki and Raymo, 2007; McKay et al., 2012).

426   The ANDRILL core, recovered in the Ross Sea sector of Antarctica, suggests that M2 is the

427   start of major cooling in Antarctica, and that this cooling is coupled with a greater instability

428   in the ice sheets (McKay et al. 2012). Antarctic ice-sheet growth around M2 is linked to the

429   beginning of expansion of the ice shelves around Antarctica (McKay et al., 2012; Riesselman

430   and Dunbar, 2013). Furthermore, a major shift in the diatom assemblage occurs just after M2,

431   with the first appearance of a number of cold water species (Riesselman and Dunbar, 2013).

432   These patterns suggest that conditions in Antarctic and in the Southern Ocean were shifting

433   towards a colder, more glaciated state through the late Pliocene, concomitant with the shift in

434   export productivity that we observed at ODP Site 1087.

435   However, we do not observe any cooling trend at ODP Site 1087 between 3.5 and 3.0

436   Ma (Figure 2), nor in sites from the northern Benguela (Rosell-Melé et al. 2014) or Subantarctic

437   Atlantic (Martinez-Garcia et al., 2010). This is opposed to the conclusions outlined in Karas et

21

438   al (2011). In that article, it was suggested that cooling in the southeast Atlantic Ocean was

439   caused by cooler waters being sent through the Indonesian Throughflow, which were then

440   translated through the Agulhas leakage, as was proposed by (Cane and Molnar, 2001).

441   However, our work shows that there was no evidence of leakage influence at this time and no

442   evidence of SST cooling between 3.5 and 3.0 Ma. This does not mean that changes in the

443   Indonesian Throughflow did not play a role, but they do not seem to have affected the record

444   between 3.5 and 3.0 Ma. It is still possible that the lack of an Agulhas Leakage at the site might

445   be linked to changes in the Indonesian Throughflow, but this would need more sites to test.

446   As a result, the shifts in export productivity at ODP Site 1087 seem unlikely to have

447   been controlled by physical changes in surface ocean hydrography. Rather, we hypothesise

448   here that the changes in export productivity could have been driven by changes to the nutrient

449   content of the waters upwelling at ODP Site 1087 through the Pliocene. This change could

450   have been either related to the total amount of nutrients delivered to the sea surface, or to the

451   actual components of the nutrients delivered to the site, as has been suggested for later periods

452   in the Benguela Upwelling where an increasing amount of Fe being delivered the subsurface

453   waters to the system in response to changing ice cover at the poles. The change in Fe led to

454   major changes in the productivity of the ocean (März et al., 2013). This resulted in an increase

455   in diatom production worldwide, including major diatom blooms in the Benguela upwelling

456   (März et al., 2013). Evidence of these diatom blooms is seen further north of the site even

457   during the Pliocene (Leduc et al., 2014). Therefore, there is previous evidence that major

458   changes in the system can be caused by changes in the nutrient content of the subsurface.

459   Since upper Antarctic Intermediate Water is a major contributor to the waters being

460   upwelled in the Benguela system, and since it forms in close association with the position of

461   the Antarctic Circumpolar Current, shifting sea surface conditions and plankton productivity

462   in the Southern Ocean might plausibly have led to a change in nutrient delivery to ODP Site

22

463   1087 after the M2 glacial. However, testing this hypothesis requires further work in detailing

464   the nutrient delivery and utilisation to Benguela sites through the Pliocene, as well as improved

465   spatial and temporal resolution data sets of changing hydrography and productivity in the

466   Southern Ocean, in order to explain the apparent decoupling between comparatively stable

467   upwelling conditions (as indicated by the SST data sets) and fluctuating biological production.

468   **5 Conclusions**

469   Our analysis of data from ODP site 1087 in the Southern Benguela region has identified

470   a displaced and/or strengthened upwelling system during the warmth of the Pliocene relative

471   to the modern. Using records of SST (U^K_{37}', TEX^H_{86}), and export productivity (stable isotopes,

472   foraminifera, alkenones and chlorins), we have shown that Pliocene SSTs remained stable and

473   were higher than modern, but that there is a stronger signal of upwelling at this site than is

474   observed during the late Pleistocene. We infer that the Benguela upwelling system was

475   displaced southward relative to present, leading to more seasonal upwelling in the northern

476   Benguela region. The Agulhas Leakage is not present in ODP Site 1087 during the Pliocene.

477   The start of Antarctic cooling and expansion of sea ice may of caused changes to the nutrient

478   delivery to the Site but did not immediately lead to any large-scale shifts in the local ocean

479   circulation. The southward displacement of the main Benguela upwelling cells during the late

480   Pliocene is consistent with the occurrence of a weaker atmospheric circulation and expanded

481   the Hadley cells in comparison to present.

482

23

493

References

495 Andrews, W.R.H., Hutchings, L., 1980. Upwelling in the Southern Benguela Current. Prog.
496   Oceanogr. 9, 1–8, IN1–IN2, 9–76, IN3–IN4, 77–81.

497 Beal, L.M., De Ruijter, W.P.M., Biastoch, A., Zahn, R., 2011. On the role of the Agulhas
498   system in ocean circulation and climate. Nature 472, 429–436.

499 Biastoch, A., Boning, C.W., Lutjeharms, J.R.E., 2008. Agulhas leakage dynamics affects
500   decadal variability in Atlantic overturning circulation. Nature 456, 489–492.
501   doi:10.1038/nature07426

502 Boebel, O., Lutjeharms, J., Schmid, C., Zenk, W., Rossby, T., Barron, C., 2003. The Cape
503   Cauldron: a regime of turbulent inter-ocean exchange. Deep. Res. Part Ii-Topical Stud.
504   Oceanogr. 50, 57–86.

505 Brierley, C.M., Fedorov, A. V, 2010. Relative importance of meridional and zonal sea
506   surface temperature gradients for the onset of the ice ages and Pliocene-Pleistocene
507   climate evolution. Paleoceanography 25, PA2214. doi:10.1029/2009pa001809

508 Brierley, C.M., Fedorov, A. V, Liu, Z., Herbert, T.D., Lawrence, K.T., LaRiviere, J.P., 2009.
509   Greatly Expanded Tropical Warm Pool and Weakened Hadley Circulation in the Early
510   Pliocene. Science (80-.). 323, 1714–1718. doi:10.1126/science.1167625

511 Caley, T., Giraudeau, J., Malaize, B., Rossignol, L., Pierre, C., 2012. Agulhas leakage as a
512   key process in the modes of Quaternary climate changes. Proc. Natl. Acad. Sci. 109,
513   6835–6839. doi:10.1073/pnas.1115545109

514 Cane, M.A., Molnar, P., 2001. Closing of the Indonesian seaway as a precursor to east
515   African aridircation around 3-4 million years ago. Nature 411, 157–162.

516 Christensen, B.A., Kalbas, J.L., Maslin, M., Murray, R.W., 2002. Paleoclimatic changes in
517   southern Africa during the intensification of Northern Hemisphere glaciation: evidence
518   from ODP Leg 175 Site 1085. Mar. Geol. 180, 117–131.

De Schepper, S., Head, M.J., Groeneveld, J., 2009. North Atlantic Current variability through marine isotope stage M2 (circa 3.3 Ma) during the mid-Pliocene. Paleoceanography 24, PA4206. doi:10.1029/2008pa001725

Dekens, P.S., Ravelo, A.C., McCarthy, M.D., 2007. Warm upwelling regions in the Pliocene warm period. Paleoceanography 22, PA3211. doi:10.1029/2006pa001394

Dowsett, H., Barron, J., Poore, R., 1996. Middle Pliocene sea surface temperatures: A global reconstruction. Mar. Micropaleontol. 27, 13–25.

Dowsett, H.J., Robinson, M.M., 2009. Mid-Pliocene equatorial Pacific sea surface temperature reconstruction: a multi-proxy perspective. Philos. Trans. R. Soc. a-Mathematical Phys. Eng. Sci. 367, 109–125. doi:10.1098/rsta.2008.0206

Dowsett, H.J., Robinson, M.M., Haywood, A.M., Hill, D.J., Dolan, A.M., Stoll, D.K., Chan, W.-L., Abe-Ouchi, A., Chandler, M.A., Rosenbloom, N.A., Otto-Bliesner, B.L., Bragg, F.J., Lunt, D.J., Foley, K.M., Riesselman, C.R., 2012. Assessing confidence in Pliocene sea surface temperatures to evaluate predictive models. Nat. Clim. Chang. 2, 365–371.

Dwyer, G.S., Chandler, M.A., 2009. Mid-Pliocene sea level and continental ice volume based on coupled benthic Mg/Ca palaeotemperatures and oxygen isotopes. Philos. Trans. A. Math. Phys. Eng. Sci. 367, 157–68. doi:10.1098/rsta.2008.0222

Emeis, K.-C., Anderson, D.M., Doose, H., Kroon, D., Schulz-Bull, D., 1995. Sea-Surface Temperatures and the History of Monsoon Upwelling in the Northwest Arabian Sea during the Last 500,000 Years. Quat. Res. 43, 355–361. doi:10.1006/qres.1995.1041

Etourneau, J., Martinez, P., Blanz, T., Schneider, R., 2009. Pliocene-Pleistocene variability of upwelling activity, productivity, and nutrient cycling in the Benguela region. Geology 37, 871–874. doi:10.1130/g25733a.1

Etourneau, J., Schneider, R., Blanz, T., Martinez, P., 2010. Intensification of the Walker and Hadley atmospheric circulations during the Pliocene-Pleistocene climate transition. Earth Planet. Sci. Lett. 297, 103–110.

Fedorov, A., Barreiro, M., Boccaletti, G., Pacanowski, R., Philander, S.G., 2007. The Freshening of Surface Waters in High Latitudes: Effects on the Thermohaline and Wind-Driven Circulations. J. Phys. Oceanogr. 37, 896–907. doi:10.1175/jpo3033.1

Fedorov, A. V, Brierley, C.M., Emanuel, K., 2010. Tropical cyclones and permanent El Nino in the early Pliocene epoch. Nature 463, 1066–1070.

Fedorov, A. V, Dekens, P.S., McCarthy, M., Ravelo, A.C., deMenocal, P.B., Barreiro, M., Pacanowski, R.C., Philander, S.G., 2006. The Pliocene paradox (mechanisms for a permanent El Nino). Science (80-.). 312, 1485–1489. doi:10.1126/science.1122666

Fietz, S., Martínez-Garcia, A., Huguet, C., Rueda, G., Rosell-Melé, A., 2011. Constraints in the application of the Branched and Isoprenoid Tetraether index as a terrestrial input proxy. J. Geophys. Res. 116, C10032. doi:10.1029/2011JC007062

25

556   Giraudeau, J., 1993. Planktonic foraminiferal assemblages in surface sediments from the
557   southwest African continental margin. Mar. Geol. 110, 47–62.

558   Giraudeau, J., Meyers, P.A., Christensen, B.A., 2002. Accumulation of organic and inorganic
559   carbon in Pliocene-Pleistocene sediments along the SW African margin. Mar. Geol. 180,
560   49–69.

561   Giraudeau, J., Pierre, C., Herve, L., 2001. A Late Quarternary, High-Resolution Record of
562   Planktonic Foraminiferal Species Distribution in the Southern Benguela Region: Site
563   1087. Proc. Ocean Drill. Program, Sci. Results .

564   Gordon, A.L., Weiss, R.F., Smethie Jr., W.M., Warner, M.J., Smethie, W.M., 1992.
565   THERMOCLINE AND INTERMEDIATE WATER COMMUNICATION BETWEEN
566   THE SOUTH-ATLANTIC AND INDIAN OCEANS. J. Geophys. Res. 97, 7223–7240.
567   doi:10.1029/92jc00485

568   Groeneveld, J., Chiessi, C.M., 2011. Mg/Ca of Globorotalia inflata as a recorder of
569   permanent thermocline temperatures in the South Atlantic. Paleoceanography 26,
570   PA2203. doi:10.1029/2010pa001940

571   Harvey, H.R., 2000. Alteration processes of alkenones and related lipids in water columns
572   and sediments. Geochemistry Geophys. Geosystems 1. doi:10.1029/2000gc000054

573   Henderiks, J., Pagani, M., 2007. Refining ancient carbon dioxide estimates: Significance of
574   coccolithophore cell size for alkenone-based pCO2 records. Paleoceanography 22,
575   PA3202. doi:10.1029/2006pa001399

576   Hernández-Sánchez, M.T., Woodward, E.M.S., Taylor, K.W.R., Henderson, G.M., Pancost,
577   R.D., 2014. Variations in GDGT distributions through the water column in the South
578   East Atlantic Ocean. Geochim. Cosmochim. Acta 132, 337–348.
579   doi:10.1016/j.gca.2014.02.009

580   Huguet, C., Schimmelmann, A., Thunell, R., Lourens, L.J., Damste, J.S.S., Schouten, S.,
581   2007. A study of the TEX(86) paleothermometer in the water column and sediments of
582   the Santa Barbara Basin, California. Paleoceanography 22, 9. doi:Pa3203
583   10.1029/2006pa001310

584   Hutchings, L., van der Lingen, C.D., Shannon, L.J., Crawford, R.J.M., Verheye, H.M.S.,
585   Bartholomae, C.H., van der Plas, A.K., Louw, D., Kreiner, A., Ostrowski, M., Fidel, Q.,
586   Barlow, R.G., Lamont, T., Coetzee, J., Shillington, F., Veitch, J., Currie, J.C., Monteiro,
587   P.M.S., 2009. The Benguela Current: An ecosystem of four components. Prog.
588   Oceanogr. 83, 15–32.

589   Jung, G., Prange, M., Schulz, M., 2014. Uplift of Africa as a potential cause for Neogene
590   intensification of the Benguela upwelling system. Nat. Geosci. advance on.
591   doi:10.1038/ngeo2249

592   Karas, C., Nurnberg, D., Tiedemann, R., Garbe-Schonberg, D., 2011a. Pliocene climate
593   change of the Southwest Pacific and the impact of ocean gateways. Earth Planet. Sci.
594   Lett. 301, 117–124.

26

595   Karas, C., Nürnberg, D., Tiedemann, R., Garbe-Schönberg, D., 2011b. Pliocene Indonesian
596   Throughflow and Leeuwin Current dynamics: Implications for Indian Ocean polar heat
597   flux. Paleoceanography 26, PA2217. doi:10.1029/2010pa001949

598   Kornilova, O., Rosell-Mele, A., 2003. Application of microwave-assisted extraction to the
599   analysis of biomarker climate proxies in marine sediments. Org. Geochem. 34, 1517–
600   1523. doi:10.1016/s0146-6380(03)00155-4

601   Leduc, G., Garbe-Schönberg, D., Regenberg, M., Contoux, C., Etourneau, J., Schneider, R.,
602   2014. The late Pliocene Benguela upwelling status revisited by means of multiple
603   temperature proxies. Geochemistry, Geophys. Geosystems 15, 475–491.
604   doi:10.1002/2013GC004940

605   Lee, K.E., Kim, J.-H., Wilke, I., Helmke, P., Schouten, S., 2008. A study of the alkenone,
606   TEX86, and planktonic foraminifera in the Benguela Upwelling System: Implications
607   for past sea surface temperature estimates. Geochemistry Geophys. Geosystems 9,
608   Q10019. doi:10.1029/2008gc002056

609   Lisiecki, L.E., Raymo, M.E., 2005. A Pliocene-Pleistocene stack of 57 globally distributed
610   benthic delta O-18 records. Paleoceanography 20, 17. doi:Pa1003
611   10.1029/2004pa001071

612   Lisiecki, L.E., Raymo, M.E., 2007. Plio-Pleistocene climate evolution: trends and transitions
613   in glacial cycle dynamics. Quat. Sci. Rev. 26, 56–69.
614   doi:10.1016/j.quascirev.2006.09.005

615   Malinverno, E., Prahl, F.G., Popp, B.N., Ziveri, P., 2008. Alkenone abundance and its
616   relationship to the coccolithophore assemblage in Gulf of California surface waters.
617   Deep Sea Res. Part I Oceanogr. Res. Pap. 55, 1118–1130.

618   Marlow, J.R., Farrimond, P., Rosell-Melé, A., 2001. Analyis of Lipid Biomarkers in
619   sedements of the Bengula Current Coastal upwelling system, in: G, W., Berger, W.H.,
620   Richter, C. (Eds.), .

621   Marlow, J.R., Lange, C.B., Wefer, G., Rosell-Mele, A., 2000. Upwelling intensification as
622   part of the Pliocene-Pleistocene climate transition. Science (80-.). 290, 2288–+.

623   Marlowe, I.T., Brassell, S.C., Eglinton, G., Green, J.C., 1984. Long chain unsaturated ketones
624   and esters in living algae and marine sediments. Org. Geochem. 6, 135–141.

625   Martínez-Botí, M.A., Foster, G.L., Chalk, T.B., Rohling, E.J., Sexton, P.F., Lunt, D.J.,
626   Pancost, R.D., Badger, M.P.S., Schmidt, D.N., 2015. Plio-Pleistocene climate sensitivity
627   evaluated using high-resolution CO2 records. Nature 518, 49–54.
628   doi:10.1038/nature14145

629   Martinez-Garcia, A., Rosell-Mele, A., Jaccard, S.L., Geibert, W., Sigman, D.M., Haug, G.H.,
630   2011. Southern Ocean dust-climate coupling over the past four million years. Nature
631   476, 312–315.

632 Martinez-Garcia, A., Rosell-Mele, A., McClymont, E.L., Gersonde, R., Haug, G.H., 2010.
633   Subpolar Link to the Emergence of the Modern Equatorial Pacific Cold Tongue. Science
634   (80-.). 328, 1550–1553. doi:10.1126/science.1184480

635 März, C., Schnetger, B., Brumsack, H.J., 2013. Nutrient leakage from the North Pacific to the
636   Bering Sea (IODP Site U1341) following the onset of Northern Hemispheric Glaciation?
637   Paleoceanography. doi:10.1002/palo.20011

638 McClymont, E.L., Ganeshram, R.S., Pichevin, L.E., Talbot, H.M., van Dongen, B.E.,
639   Thunell, R.C., Haywood, A.M., Singarayer, J.S., Valdes, P.J., 2012. Sea-surface
640   temperature records of Termination 1 in the Gulf of California: Challenges for seasonal
641   and interannual analogues of tropical Pacific climate change. Paleoceanography 27,
642   PA2202. doi:10.1029/2011pa002226

643 McClymont, E.L., Rosell-Mele, A., Giraudeau, J., Pierre, C., Lloyd, J.M., 2005. Alkenone
644   and coccolith records of the mid-Pleistocene in the south-east Atlantic: Implications for
645   the U-37(K) index and South African climate. Quat. Sci. Rev. 24, 1559–1572.
646   doi:10.1016/j.quascirev.2004.06.024

647 McKay, R., Naish, T., Carter, L., Riesselman, C., Dunbar, R., Sjunneskog, C., Winter, D.,
648   Sangiorgi, F., Warren, C., Pagani, M., Schouten, S., Willmott, V., Levy, R., DeConto,
649   R., Powell, R.D., 2012. Antarctic and Southern Ocean influences on Late Pliocene
650   global cooling. Proc. Natl. Acad. Sci. 109, 6423–6428. doi:10.1073/pnas.1112248109

651 Müller, P.J., Kirst, G., Ruhland, G., von Storch, I., Rosell-Mele, A., 1998. Calibration of the
652   alkenone paleotemperature index U-37(K ') based on core-tops from the eastern South
653   Atlantic and the global ocean (60 degrees N-60 degrees S). Geochim. Cosmochim. Acta
654   62, 1757–1772.

655 Passchier, S., 2011. Linkages between East Antarctic Ice Sheet extent and Southern Ocean
656   temperatures based on a Pliocene high-resolution record of ice-rafted debris off Prydz
657   Bay, East Antarctica. Paleoceanography 26, PA4204. doi:10.1029/2010pa002061

658 Peeters, F.J.C., Acheson, R., Brummer, G.-J.A., de Ruijter, W.P.M., Schneider, R.R.,
659   Ganssen, G.M., Ufkes, E., Kroon, D., 2004. Vigorous exchange between the Indian and
660   Atlantic oceans at the end of the past five glacial periods. Nature 430, 661–665.

661 Pierre, C., Saliege, J.F., Urrutiaguer, M.J., Giraudeau, J., 2001. Stable isotope record of the
662   last 500 k.y. at Site 1087 (Southern Cape Basin). Proc. ODP, Sci. Results.

663 Prell, W.L., 1984. Covariance Patterns of Foraminiferal $\delta18O$: An Evaluation of Pliocene Ice
664   Volume Changes Near 3.2 Million Years Ago. Science (80-.). 226, 692–694.
665   doi:10.1126/science.226.4675.692

666 Riesselman, C.R., Dunbar, R.B., 2013. Diatom evidence for the onset of Pliocene cooling
667   from AND-1B, McMurdo Sound, Antarctica. Palaeogeogr. Palaeoclimatol. Palaeoecol.
668   369, 136–153. doi:10.1016/j.palaeo.2012.10.014

669 Rosell-Melé, A., Martínez-Garcia, A., McClymont, E.L., 2014. Persistent warmth across the
670   Benguela upwelling system during the Pliocene epoch. Earth Planet. Sci. Lett. 386, 10–
671   20. doi:10.1016/j.epsl.2013.10.041

672 Rosell-Melé, A., Maxwell, J.R., 1996. Rapid Characterization of Metallo Porphyrin Classes
673   in Natural Extracts by Gel Permeation Chromatography/Atmospheric Pressure Chemical
674   Ionization/Mass Spectrometry. Rapid Commun. Mass Spectrom. 10, 209–213.
675   doi:10.1002/(sici)1097-0231(19960131)10:2<209::aid-rcm462>3.0.co;2-u

676 Schouten, S., Hopmans, E.C., Schefuss, E., Damste, J.S.S., 2002. Distributional variations in
677   marine crenarchaeotal membrane lipids: a new tool for reconstructing ancient sea water
678   temperatures? (vol 204, pg 265, 2002). Earth Planet. Sci. Lett. 204, 265–274.

679 Seki, O., Foster, G.L., Schmidt, D.N., Mackensen, A., Kawamura, K., Pancost, R.D., 2010.
680   Alkenone and boron-based Pliocene pCO2 records. Earth Planet. Sci. Lett. 292, 201–
681   211.

682 Sexton, P.F., Norris, R.D., 2011. High latitude regulation of low latitude thermocline
683   ventilation and planktic foraminifer populations across glacial-interglacial cycles. Earth
684   Planet. Sci. Lett. 311, 69–81. doi:10.1016/j.epsl.2011.08.044

685 Shaari, H. bin, Yamamoto, M., Irino, T., 2013. Enhanced upwelling in the eastern equatorial
686   Pacific at the last five glacial terminations. Palaeogeogr. Palaeoclimatol. Palaeoecol.
687   386, 8–15. doi:10.1016/j.palaeo.2013.03.022

688 Shipboard Scientific Party, Party, S.S., 1998. Site 1087, in: Wefer Berger, W.H., Richter, C.,
689   et al., G. (Ed.), Proc. ODP, Init. Repts. Ocean Drilling Program, College Station, TX,
690   pp. 457–484.

691 Ufkes, E., Jansen, J.H.F., Schneider, R.R., 2000. Anomalous occurrences of
692   Neogloboquadrina pachyderma (left) in a 420-ky upwelling record from Walvis Ridge
693   (SE Atlantic). Mar. Micropaleontol. 40, 23–42.

694 Ufkes, E., Kroon, D., 2012. Sensitivity of south-east Atlantic planktonic foraminifera to mid-
695   Pleistocene climate change. Palaeontology 55, 183–204. doi:10.1111/j.1475-
696   4983.2011.01119.x

697 Volkman, J.K., Eglinton, G., Corner, E.D.S., Forsberg, T.E. V, 1980. Long-chain alkenes and
698   alkenones in the marine coccolithophorid Emiliania huxleyi. Phytochemistry 19, 2619–
699   2622.

700 Wang, D., Gouhier, T.C., Menge, B.A., Ganguly, A.R., 2015. Intensification and spatial
701   homogenization of coastal upwelling under climate change. Nature 518, 390–394.
702   doi:10.1038/nature14235

703 Weijer, W., De Ruijter, W.P.M., Dijkstra, H.A., 2001. Stability of the Atlantic Overturning
704   Circulation: Competition between Bering Strait Freshwater Flux and Agulhas Heat and
705   Salt Sources. J. Phys. Oceanogr. 31, 2385–2402. doi:10.1175/1520-
706   0485(2001)031<2385:sotaoc>2.0.co;2

707   Ziveri, P., Stoll, H., Probert, I., Klaas, C., Geisen, M., Ganssen, G., Young, J., 2003. Stable
708   isotope "vital effects" in coccolith calcite. Earth Planet. Sci. Lett. 210, 137–149.
709   doi:10.1016/S0012-821X(03)00101-8

710

711

712

713

714

715